MÖSSBAUER EFFECT INVESTIGATIONS OF THE MAGNETIC PROPERTIES OF SINGLE CRYSTAL THULIUM ETHYLSULPHATE

Thesis by
Frank T. Snively

In Partial Fulfillment of the Requirements
For the Degree of
Doctor of Philosophy

California Institute of Technology
Pasadena, California
1965
(Submitted May 26, 1965)

ACKNOWLEDGEMENTS

Many people have provided some assistance to the author during the course of this work. Particular thanks are due to the following:

Dr. Rudolf L. Mössbauer for his advice and assistance in many aspects of this work.

Dr. F. H. Spedding, of the Iowa State University, for his very kind donation of the thulium ethylsulphate single crystals used in the experiments.

Dr. Egbert Kankeleit for his frequent assistance, especially with the velocity transducers and electronics used in the experiments.

Dr. Felix H. Boehm, for his successful efforts to produce an atmosphere conductive to creative scientific work.

Dr. Sten Samson, for loan of equipment and expert knowledge in the X-ray analysis of the single crystals.

Mr. M. J. Clauser, who provided several of the computer programs used in the analysis of the data.

Mr. H. E. Henrickson, for his advice and assistance in the design of various pieces of apparatus.

Finally, I would particularly like to thank Mr. Vaughn Stephenson and Mr. Ellsworth "Woody" Kiersey, for their help in building many parts of the apparatus used here. Their ability to turn a vaguely expressed wish into a smoothly functioning piece of hardware was of great benefit in performing the experiments.

This work was supported in part by the U. S. Atomic Energy Commission.

ABSTRACT

Mössbauer effect experiments have been performed on a single crystal of paramagnetic thulium ethylsulphate with a magnetic field applied. The effect of the electric field of the surrounding ligands in the crystal, as determined from published optical spectroscopic data, combined with the effect of an externally applied magnetic field, has been used to compute the electron wave function of the thulium ion, yielding, within numerical factors, the electric field gradient and magnetic field at the nucleus. The nuclear hyperfine splittings and transition intensities were computed as a function of the ratio of quadrupole interaction energy to the magnetic interaction energy for magnetic fields parallel and perpendicular to the (zz) axis of the electric field gradient tensor. The results of these calculations have been compared with experiment. It has been found that the ratio of internal magnetic field to external magnetic field varies by a factor of at least 35 as the orientation of the crystal is changed. When the field was applied perpendicular to the z-direction, which gave the maximum internal field, the ratio of internal to external field was found to be 73 ± 7 at $6.5\ ^{o}K$. Our most significant result is the measurement by a new technique, of the radial integral appearing in the nuclear magnetic hyperfine interaction $\langle r^{-3} \rangle_{M}$. The numerical value was found to be $\langle r^{-3} \rangle_{M} = 11.1 \pm 1.0$ atomic units. Other possible applications of the use of magnetic fields with rare earth single crystals in Mössbauer effect investigations are discussed.

TABLE OF CONTENTS

I. INTRODUCTION

The phenomenon of recoilless nuclear resonance (Mössbauer effect) provides a convenient tool for the study of the interactions between a nucleus and its surroundings. In appropriately designed experiments, one may obtain quite detailed information about the charge distribution and magnetic fields within the ion in which the nucleus resides, and from this infer various properties of the ion and its surroundings in the crystal.

In this thesis, we report the first observations using the Mössbauer effect of the nuclear hyperfine splittings which result from the application of a magnetic field to a paramagnetic single crystal. Specifically, we have studied the hyperfine interaction of tripositive thulium in the ionic salt thulium ethylsulphate (TmES). The radial integral factor appearing in this interaction, which is $\langle r^{-3} \rangle$ taken over the 4-f electrons, has been determined.

In contrast to other experiments, our measurement is relatively free from sources of systematic uncertainty. Most determinations of this radial integral involve measurements either on a neutral atom in an atomic beam or on the (presumably) ionized atom in a ferromagnetic metal. The atomic beam measurements are, of course, quite precise, but they give $\langle r^{-3} \rangle$ only for neutral atoms, and values for trivalent can only be obtained very indirectly. On the other hand, the inference of $\langle r^{-3} \rangle$ from data taken with the ferromagnetic metals is quite uncertain because such materials contain conduction electrons of unknown polarization. The polarized conduction electrons may contribute appreciably to the nuclear magnetic interaction and lead to considerable systematic error. The

difficulties inherent in both of these methods are circumvented by our special method of studying the behavior of an ionic salt.

A measurement using the Mössbauer effect can give the electric field gradient (EFG) and the magnetic field at the nucleus. We can understand the origin of these fields in the following way: The rare earth ion has a partially filled 4-f electron shell. As a result of spin-orbit coupling, the ion is split into states characterized by the total angular momentum. When the ion is put into a crystal, the lowest multiplet state (which was degenerate with respect to the projection of the angular momentum) undergoes a Stark effect splitting by the electric field in the crystal. This gives a series of levels, the crystalline electric field, or CEF, levels, which have an overall splitting of a few hundred cm^{-1}. The overall splitting is small compared with the spin-orbit coupling energy, so that higher multiplet levels are not mixed, and the total angular momentum remains a good quantum number.

The magnetic behavior of the rare earth salts can be described with phenomenological theories. The angular part of the matrix elements that are associated with the interactions of a particular ion with crystal electric fields and external magnetic fields is handled by angular momentum algebra, but there are no reliable methods for calculating the necessary radial integrals; the uncertainty in such calculations is typically around 30%. It is therefore customary to treat these radial integrals as parameters, which are to be determined by experiment. There is, accordingly, a considerable need for reliable determination of such quantities,both because numerical values are required in any magnetic calculation, and because theoretical estimates can be best improved by the "feedback" of experimental results.

In the case of thulium, which has an even number of electrons in the tripositive ion (no Kramers degeneracy),the CEF levels usually have no intrinsic magnetic moment. The occurrence of magnetic susceptibility then depends on the fact that a magnetic field can admix to a particular CEF level appreciable amplitudes from other CEF levels, which results in a nonzero magnetization. This phenomenon often shows up most clearly at low temperatures: when the temperature is low enough that only the lowest CEF level is appreciably populated, the susceptibility depends only on the amplitude admixtures, and not on the temperatures. This phenomenon of susceptibility which approaches a constant value at low temperature is called "Van Vleck temperature independent susceptibility".

The nuclear quadrupole moment interacts with the electric field gradient from the CEF levels and from the surrounding lattice, and the nuclear magnetic moment interacts with magnetic fields which may be present. We observe both types of hyperfine interaction.

The strength of the magnetic field at the nuclear position has been determined from experiment as a function of orientation. The exact form of the CEF states for TmES was derived from optical spectroscopic data by Barnes, et al.[1] The effect of a magnetic field on these states has been calculated in this thesis, giving the magnetic moment per atom as a function of field strength and orientation with respect to the crystal axes. Comparison of these quantities with our experimental results yields the strength of the nuclear magnetic hyperfine interaction.

Since the salt being studied does not have any spontaneous magnetic ordering, it is necessary to apply an external magnetic field to produce polarization of the atoms.

The electrons responsible for magnetic polarization interact with the anisotropic CEF, as well as the magnetic field; the polarization will, in all likelihood, be anisotropic. Because of this anisotropy, it is necessary to use a single crystal.

The Mössbauer level used was the 8.4 keV state in Tm^{169}. The choice of this particular level was based on the following considerations:

(1) The spins of the ground state ($I = 1/2$) and of the excited state ($I = 3/2$) are relatively low, which results in a small number of hyperfine lines in the observed spectra, which considerably simplifies the interpretation of the experimental data.

(2) The recoil-free fraction (Debye-Waller factor) is quite high, due to the low energy of the transition; thus, one may perform experiments over a wide range of temperatures without encountering serious difficulties due to small resonance effects.

(3) The isotopic abundance of Tm^{169} is 100%.

(4) It is relatively easy to prepare radioactive sources of high specific activity which emit a single line, thus facilitating the study of various absorbers[1].

II. THE ORIGIN OF THE INTERNAL FIELDS

The hamiltonian describing the interactions of the nuclear electric quadrupole moment and magnetic dipole moment with the surroundings may be written as

$$H = H_Q + H_M \ , \tag{1}$$

where the quadrupole part, H_Q is

$$H_Q = \frac{e^2Q}{4I(2I-1)} \left[\langle q_{zz} \rangle (3\underset{\sim}{I}_z^2 - \underset{\sim}{I}^2) + \frac{1}{2} \langle q_{xx} - q_{yy} \rangle (I_+^2 + I_-^2) \right], \tag{2}$$

and the magnetic part H_M is

$$H_M = \frac{-g_N \mu_N}{I} (\underset{\sim}{I} \cdot \underset{\sim}{H}_{int}) \ . \tag{3}$$

(In these equations, Q in the nuclear quadrupole moment, $\langle q_{ii} \rangle$ are the non-vanishing components of the electric field gradient tensor, $\underset{\sim}{I}$ is the nuclear spin operator, $g_N \mu_N$ is the nuclear magnetic moment, and $\underset{\sim}{H}_{int}$ is the magnetic field at the nuclear position). We have chosen a co-ordinate system lying along the principal axes of the electric field gradient (EFG) tensor. We discuss the terms appearing in Equations (2) and (3) below.

(1) Quadrupole interaction

This interaction has been discussed thoroughly in a recent publication[1]; we summarize a few of the pertinent results here.

The electric field gradient at the nucleus arises from two distinct sources, namely the gradients of the electrostatic field of the surrounding ligands in the crystal, and the field gradient at the nuclear position due to the electrons in the atom in question. More specifically, we write the EFG tensor q_{ij} as

$$q_{ij} = (1 - \gamma_\infty)q_{ij}^{Lat} + (1 - R_Q)q_{ij}^{4f} \quad . \tag{4}$$

The meaning of the terms is as follows: the field gradient of the surrounding ligands, q_{ij}^{Lat} polarizes the closed shells of the thulium atom, producing a quadrupole distortion which alters the EFG which appears at the nucleus. The term γ_∞ represents the effect of this polarization. The partially filled 4-f electron shell produces an EFG, q_{ij}^{4f} at the nucleus also; a quadrupole polarization of the closed shells can be produced by this contribution as well. The factor R_Q represents the shielding due to this polarization.

The EFG is temperature dependent. The overall splitting of the ground state multiplet of thulium due to the electric fields of the surrounding ligands (called the crystalling electric field, or CEF) is typically 200 to 300 cm^{-1}. Thus, the populations of the sublevels change considerably as one goes from liquid helium temperature up to room temperature, giving a strong temperature dependence for q_{ij}^{4f}. On the other hand, the lattice part of the EFG depends only on positions, polarizibilities, and charges of the surrounding ligands, so we expect only a slight temperature variation.

The calculation of q_{ij}^{4f} depends on a knowledge of the electronic states in the ground state multiplet. Assuming that the total angular momentum, J, is a good quantum number, we have the following equation for the matrix elements of the CEF hamiltonian:

$$(H_{CEF})_{m_J, m_J'} = \sum_{n,m} C_n^m \langle J \| \theta_n \| J \rangle \langle J, m_J | O_n^m(\underset{\sim}{J}) | J, m_J' \rangle \quad , \qquad (5)$$

where the C_n^m are products of coefficients for the spherical harmonic expansion of the CEF multiplied by appropriate integrals over the radial distribution of the 4-f electrons, and $\langle J \| \theta_n \| J \rangle$ are reduced matrix elements appropriate to the equivalent operators $O_n^{m\ (2)}$. If the CEF hamiltonian is put into diagonal form, we obtain a series of eigenstates which we label as

$$H_{CEF} | \lambda \rangle = E_\lambda | \lambda \rangle \quad . \qquad (6)$$

Representing these states in the coordinate system of the principal axes of the EFG tensor, we obtain explicit expressions for the q_{ii}^{4f}:

$$\langle q_{zz} \rangle = - \langle r^{-3} \rangle \langle J \| \theta_2 \| J \rangle \langle \lambda | 3\underset{\sim}{J}_z^2 - \underset{\sim}{J}^2 | \lambda \rangle \quad , \qquad (7a)$$

$$\langle q_{xx} - q_{yy} \rangle = -3/2 \langle r^{-3} \rangle \langle J \| \theta_2 \| J \rangle \langle \lambda | J_+^2 + J_-^2 | \lambda \rangle \quad . \qquad (7b)$$

In the absence of shielding effects, $\langle r^{-3} \rangle$, would be simply the integral of r^{-3} over the 4-f radial distribution. However, we choose instead to treat the quantity $\langle r^{-3} \rangle_Q$, defined by the equation

$$\langle r^{-3} \rangle_Q = (1 - R_Q) \langle r^{-3} \rangle \quad , \tag{8}$$

as a parameter to be determined by experiment.

The temperature variation of q_{ii}^{4f} can be obtained by taking thermal averages over the expectation values defined in Equations (7a) and (7b). The nuclear quadrupole interaction (Equation 2) retains the same form provided we use the appropriate thermal averages $\langle q_{ii}^{4f} \rangle_T$ in the equation.

(2) Magnetic interactions

The magnetic fields at the nuclear position in the rare earths are quite large (typically several million gauss), so that it is possible to neglect the direct interaction of the nucleus with external magnetic fields or with fields produced by neighboring paramagnetic ions in comparison with the fields produced by the electrons in the atom itself. We may accordingly treat the internal field as arising from a two step process: the atom becomes magnetically polarized by external means and the polarization leads to a certain internal field. Since the magnetic moment of Tm atom is given in terms of the total angular momentum vector by

$$\underset{\sim}{M} = g_J \mu_B \langle \underset{\sim}{J} \rangle \quad , \tag{9}$$

where g_J is the Landè factor, and μ_B is the Bohr magneton, it suffices to examine $\langle \underset{\sim}{J} \rangle$ under various conditions of interest. In our case of Tm in TmES, where the CEF levels all have $\langle \underset{\sim}{J} \rangle = 0$ in the absence of an applied field, we may simply treat the magnetization as arising from the interaction of the atom with the

external magnetic field. The details of the calculation of this magnetization are discussed in the next chapter.

The magnetic field at the nucleus in terms of the spin and orbital angular momenta of the electrons in the atom is given by[3]

$$H_{int} = 2\mu_B \sum_i \frac{(\underset{\sim}{\ell}_i - \underset{\sim}{s}_i)}{r_i^3} + \frac{3\underset{\sim}{r}_i(\underset{\sim}{s}_i \cdot \underset{\sim}{r}_i)}{r_i^5} + \frac{8\pi}{3}\underset{\sim}{s}_i \delta(\underset{\sim}{r}_i) \quad , \tag{9}$$

where ℓ_i is the orbital angular momentum, s_i the spin, and r_i the position of the i'th electron. Since all the quantities in the above equation transform like a vector under rotation of the coordinates, we may replace this equation, within the manifold of states spanned by the vector J, as

$$\underset{\sim}{H}_{int} = 2\mu_B \langle J||N||J\rangle \langle r^{-3}\rangle_M \langle \underset{\sim}{J}\rangle \quad , \tag{10}$$

where $\langle J||N||J\rangle$ is a reduced matrix element, whose numerical value for Tm^{+++} is 7/9. Due to the fact that the magnetically polarized 4-f electrons can interact with the filled shells, the quantity $\langle r^{-3}\rangle_M$ is not simply the expectation value of this quantity taken over the 4-f electrons only. Additional orbital contributions to the internal field arise from the mixing of electronic states with different ℓ. Exchange interactions involving the spins can give a nonzero net spin at the nucleus, thus giving a magnetic interaction via the Fermi contact term $\frac{8\pi}{3}\underset{\sim}{s}_i \delta(\underset{\sim}{r}_i)$. The orbital mixing is proportional to $\underset{\sim}{L}$, the total orbital angular momentum, and the spin mixing is proportional to $\underset{\sim}{S}$, the total spin, and since both of these quantities are proportional to $\underset{\sim}{J}$ when Russell-Saunders coupling applies (as it does in

the case of Tm), we can represent the combined effect of the closed shell polarizations by defining a magnetic shielding factor R_M. This factor is independent (in the Russell-Saunders coupling limit) of the exact value of $\langle \underset{\sim}{J} \rangle$, and is another constant of proportionality in the definition of $\underset{\sim}{H}_{int}$. In analogy with the quadrupole coupling case, we are led to define an effective $\langle r^{-3} \rangle_M$ which includes the magnetic shielding factor:

$$\langle r^{-3} \rangle_M = (1 - R_M) \langle r^{-3} \rangle_{4f} \quad . \tag{11}$$

In the experiments reported on here, the quantity $\langle r^{-3} \rangle_M$ is determined from a measurement of the internal field and a calculation of $\langle \underset{\sim}{J} \rangle$, using Equations (3) and (10).

III. CALCULATION OF THE INTERNAL FIELDS IN TmES

The ethylsulphate $Tm(C_2H_5SO_4)_3 \cdot 9H_2O$ was selected for these experiments because it is the only thulium salt with a simple electronic structure which has been thoroughly studied by optical spectroscopy. Accordingly, the effect of a magnetic field can be calculated with confidence.

The magnetic field at a particular atom is given by the vector sum of the magnetic field applied externally and the magnetic field due to the induced dipole moments of the surrounding atoms. In our case, the crystal is in the form of a thin plate with the external field lying in the plane of the plate, so that the correction for depolarizing fields is negligible. An explicit calculation[4] has shown that the field at a particular atomic site due to the surrounding dipoles is small. Accordingly, we write the field at a particular ion H_{loc} as:

$$H_{loc} = H_{applied}(1 + \frac{4\pi}{3} \chi) \quad , \tag{12}$$

where χ is the susceptibility. The experimentally determined susceptibility[5] at 0 ^{o}K is about 2×10^{-3}, so the field at the Tm atom is only a per cent larger than the applied field. We now investigate the effects of the field.

The qualitative features of the paramagnetic behavior are best illustrated with the aid of the CEF level diagram (Table I). When the field is parallel to the symmetry axis of the crystal, admixtures to the lowest state can only be produced by matrix elements of J_z. States which can be so admixed lie at fairly high energy, so that the admixture is small. We accordingly expect the effect of an external field to be relatively small. On the other

TABLE 1

Energies, wave functions and electric field gradients of the CEF levels of the $^3H_6$ term of the ground multiplet of thulium ethyl sulphate (C_{3h} symmetry), using the CEF parameters and the reduced matrix elements given in reference (1). (Energies are in cm^{-1}.)

Energy	Degeneracy	Wave Function[a]
300.1	1	$-0.707\|-3\rangle + 0.707\|+3\rangle$
273.6	2	$-0.446\|-2\rangle + 0.895\|+4\rangle$
		$0.895\|-4\rangle - 0.446\|+2\rangle$
221.0	1	$0.697\|-6\rangle - 0.168\|0\rangle + 0.697\|+6\rangle$
214.8	1	$-0.707\|-6\rangle + 0.707\|+6\rangle$
148.1	2	$-0.305\|-1\rangle + 0.953\|+5\rangle$
		$-0.953\|-5\rangle + 0.305\|+1\rangle$
157.1	1	$0.707\|-3\rangle + 0.707\|+3\rangle$
110	2	$0.895\|-2\rangle + 0.446\|+4\rangle$
		$0.446\|-4\rangle + 0.895\|+2\rangle$
31.3	2	$0.305\|-5\rangle + 0.953\|+1\rangle$
		$0.953\|-1\rangle + 0.305\|+5\rangle$
0	1	$0.119\|-6\rangle + 0.986\|0\rangle + 0.119\|+6\rangle$

a The general form of the wave function is as defined in Equations (6) and (7).

hand, the application of a magnetic field perpendicular to the symmetry axis involves matrix elements of J_+ and J_-. These operators can admix the first excited level (which happens by accident to be doubly degenerate) into the ground state. We accordingly expect the magnetic effects to be relatively large. This is indeed found to be the case. Illustration 1 shows three spectra, taken at 6.5 ^{O}K with no field, field parallel to the c-axis, and field perpendicular to the c-axis. A comparison of the spectra demonstrates the anisotropy of the magnetic effect. The anisotropy is discussed in greater detail in Chapter VI.

We now describe the method for explicit calculation of the magnetic effect: the matrix elements for the 4-f electrons in (J, m_J) representations are given by

$$H_{m_J, m'_J} = (H_{CEF})_{m_J, m'_J} - \mu_B g_J \langle m_J | \underset{\sim}{J} \cdot \underset{\sim}{H} | m'_J \rangle \quad , \tag{13}$$

where H_{CEF} is given by Equation (4). The symmetry of the CEF determines the number of independent parameters which can be used to characterize the CEF Hamiltonian. In the case of the TmES, where the point symmetry for the Tm ions is C_{3h}, there are four such parameters if appropriate co-ordinate axes are chosen. The coordinate system has a simple relation to the external symmetry of the crystal, which is hexagonal. The Z-axis lies along the hexagonal axis, the X-axis passes nearly through an edge of the hexagonal prism, and the Y-axis is nearly perpendicular to a face.

For problems such as ours, in which the sign of the magnetic field does not matter, there are six equivalent directions in which the X- and Y-axes may be put. If we choose one of these for our

ILLUSTRATION 1

Mössbauer spectra taken with no external magnetic field, a field of 2000 gauss parallel to the hexagonal axis of the crystal, and a field of 2000 gauss perpendicular to the hexagonal axis. All three spectra were taken at the same temperature.

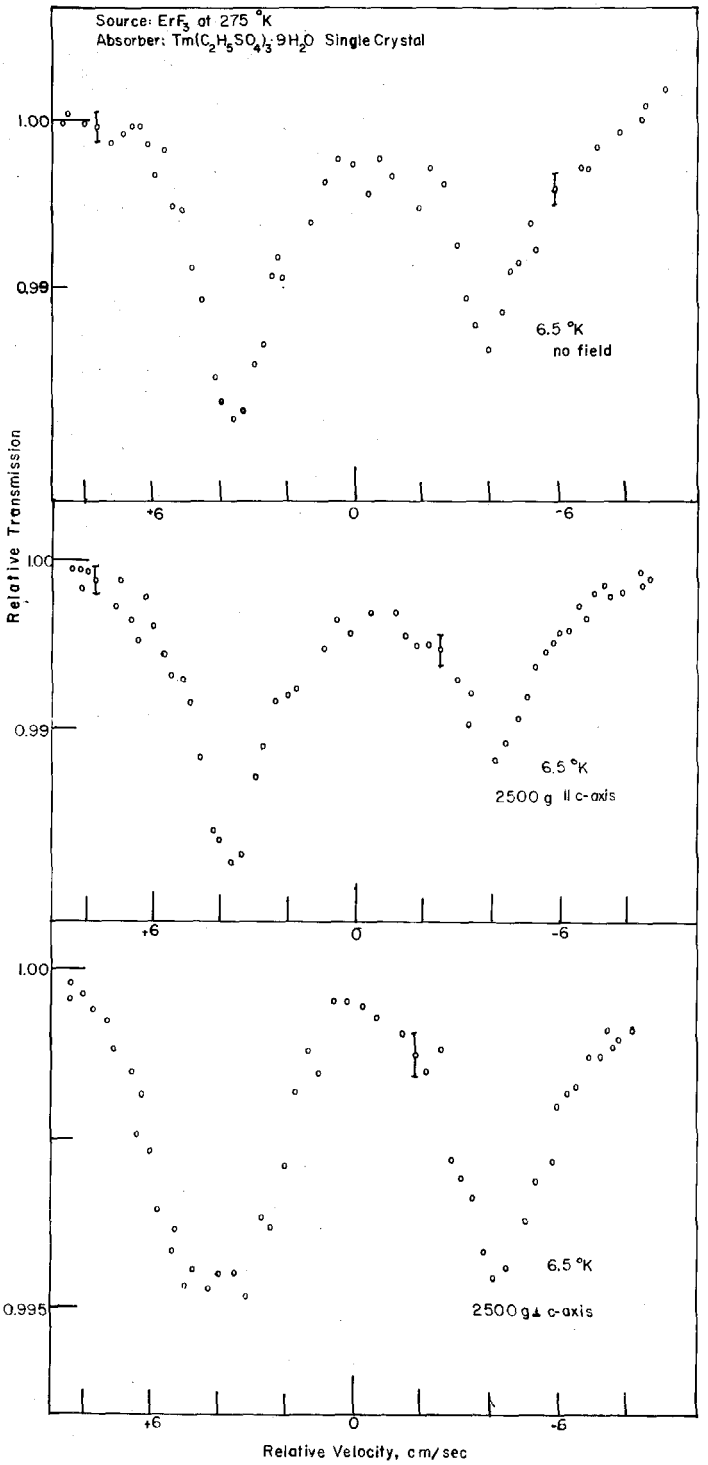
Source: ErF_3 at 275 °K
Absorber: $Tm(C_2H_5SO_4)_3 \cdot 9H_2O$ Single Crystal
1.00
0.99
6.5 °K
no field
+6
0
-6
Relative Transmission
1.00
0.99
6.5 °K
2500 g ∥ c-axis
+6
0
-6
1.00
0.995
6.5 °K
2500 g ⊥ c-axis
+6
0
-6
Relative Velocity, cm/sec

co-ordinate system, we may write the magnetic part of Equation (13) in the form

$$(H_{mag})_{m_J, m'_J} = g_J \mu_B H \langle m_J | \underset{\sim}{J} \cdot \underset{\sim}{e}_H | m'_J \rangle \ , \qquad (14)$$

where $\underset{\sim}{e}_H$ is a unit vector in the direction of the external magnetic field. It is useful to examine the magnitude of certain quantities in order to estimate the overall effect of the magnetic field on the CEF levels. Taking a typical magnetic field matrix element to have numerical value 6, and a magnetic field strength of 10^4 gauss we obtain

$$g_J \mu_B H \langle m_J | J_{typ} | m'_J \rangle \approx 3.3 \text{ cm}^{-1} . \qquad (15)$$

This quantity must be compared with the overall CEF splitting of 300 cm^{-1}, and a typical energy denominator (in a perturbation-theoretic calculation) of 30 cm^{-1} to 50 cm^{-1}. We may expect typical amplitude admixtures to be of the order of a few per cent, and it seems clear that any magnetic effect may be treated as a perturbation on the CEF levels as long as the field is smaller than, or comparable to, 10 kilogauss. The magnetic moment per atom per unit field strength has been calculated by treating the magnetic field as a perturbation on the CEF levels shown in Table 1. The calculated variation of the moment with temperature is in substantial agreement with the experimental results of Gerstein et al.[10], when the field is in the x-direction, although for the z-axis case, we calculate a somewhat smaller moment than is measured. The latter disagreement is probably due to experimental difficulty in measuring the small z-axis susceptibility. The explicit form of the lowest

CEF level, (from which $\langle \underset{\sim}{J} \rangle$ may be calculated) when the field is in the x-direction, is

$$|g\rangle = 0.12|-6\rangle + 5.5 \times 10^{-8}H|-5\rangle + 5.1 \times 10^{-6}H|-1\rangle + 0.99|0\rangle + 5.1 \times 10^{-6}H|1\rangle + 1.6 \times 10^{-7}H|5\rangle + 0.12|6\rangle , \quad (16)$$

where H is the applied field in Oersteds. It can be seen that a field of a few k0er gives an amplitude admixture of a few per cent, so that the use of perturbation theory is certainly justified.

IV. THE NUCLEAR ENERGIES AND TRANSITIONS INTENSITIES

When the ethylsulphate is put in a magnetic field, the nucleus is subject to the combined effect of the electric field gradient and the internal magnetic field. The ground state of Tm, with $I = 1/2$, is split by the magnetic field into two states, whose separation is

$$\Delta E_g = 2 g_g \mu_N H_{int} \quad . \tag{17}$$

However, the excited state is split into four levels, which are equally spaced only in the limit of zero quadrupole interaction. The splittings, which result from an axially symmetric field gradient combined with a magnetic field, are dependent on both the strength of the magnetic field and on the direction in which the field is applied. The complete expression for the nuclear interaction in the excited state is given by the matrix elements of the hamiltonian

$$H_{nuc} = \frac{e^2 Q V_{zz}}{4I(2I-1)} (3\underset{\sim}{I}_z^2 - \underset{\sim}{I}^2) + \frac{g \mu_N}{I} \underset{\sim}{H}_{int} \cdot \underset{\sim}{I} \quad , \tag{18}$$

where the vector $\underset{\sim}{I}$ is the nuclear spin operator, and the terms V_{zz} and H_{int} are defined in Equations (4) and (10).

When the field is in the z-direction the splitting is simple. As the magnetic field increases, the states separate in a linear fashion into 4 levels characterized by the eigenvalues of I_z. This behavior is shown in Illustration 2a. When the field is in the x-direction, the result is more complicated, and numerical computation is necessary. Illustration 2b shows the results of such a computation when the ratio of magnetic energy to electric quadrupole energy,

ILLUSTRATION 2

The energy of the first excited state of Tm^{169} resulting from an electric field gradient and a magnetic field in the direction indicated. The Field Strength Ratio, defined in Chapter 5, measures the strength of the magnetic interaction energy with respect to the quadrupole interaction energy. The energy scale is the same for both sets of curves, but otherwise is arbitrary. The curves in the lower half of the illustration have labels to specify the individual hyperfine levels.

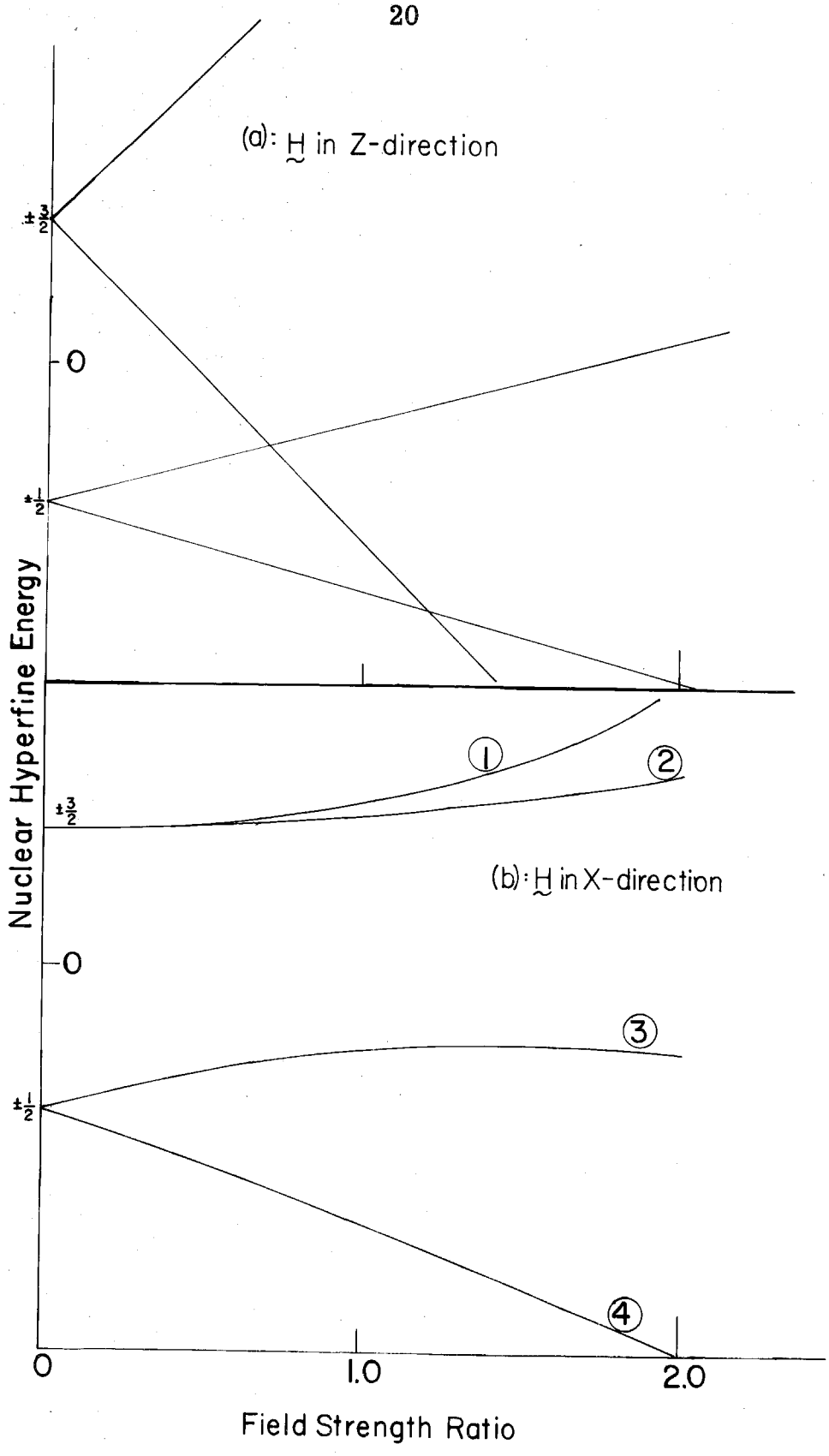
(a): H in Z-direction
±3/2
0
±1/2
Nuclear Hyperfine Energy
①
②
±3/2
(b): H in X-direction
0
③
±1/2
④
0
1.0
2.0
Field Strength Ratio

(the "field strength ratio") is ≤ 2. In either case, the positions of the observed Mössbauer absorption peaks are determined by the splittings of the ground and excited levels. The analysis of an observed spectrum requires a knowledge of the intensities, as well as the energies, of the transitions. The intensities are not the same as those which are found with polycrystalline absorber and they vary with field strength, so a separate calculation is necessary. As an additional complication the nuclear hyperfine levels are not, in general, eigenfunctions of I_z, the z component of the nuclear spin operator. We must, accordingly, represent a typical hyperfine state in the form (m = eigenvalue of I_z):

$$|\alpha\rangle = \sum_{m} a_{\alpha m} |m\rangle \quad . \tag{19}$$

Assuming that the radiation is of magnetic dipole character, we have the following expression for the intensity of radiation in a direction given by spherical angles (θ, φ), and with linear polarization at angle ψ [5]:

$$I_{\alpha\to\beta}(\theta, \varphi, \psi) = \frac{3\pi^2}{2} |\langle \text{exc}\|M1\|\text{gnd}\rangle|^2 \times \Big|\sum_{m'} \sum_{M=-1}^{1} \sum_{P=\pm 1} a_{\alpha m'} a_{\beta m} e^{-iP\psi}$$

$$\times D^1_{MP}(\theta, \varphi, 0)\, C(3/2,\ 1,\ 1/2;\ m',\ M,\ m)\Big|^2 \quad , \tag{20}$$

where $\langle \text{exc}\|M1\|\text{gnd}\rangle$ is a reduced matrix element giving the transition rate from the excited state to the ground state, $a_{\alpha m'}$ and $a_{\beta m}$ are amplitudes for the projection of I_z in the excited state and ground state, respectively, $D^1_{MP}(\theta, \varphi, 0)$ is the rotation operator of order 1, and $C(3/2,\ 1,\ 1/2;\ m',\ M,\ m)$ is a Clebsch-Gordan coefficient, with

M representing the Δm change in the transition. Since the polarization is not measured in the experiment, it is necessary to average over polarization angles to obtain the final intensity. Note especially that the polarization index "P" appears in the rotation operator, so that interference between circular polarizations can occur. This has the practical effect that the explicit form of the sum appearing above is exceedingly complicated, and very little can be said in detail about the expressions which result. We particularize to the case of interest here, namely observation in the negative y-direction when the field is applied in the x-direction, using the co-ordinate system of Chapter III. It is found that in the limiting cases when either the quadrupole interaction or the magnetic hyperfine interaction vanishes that two of the transition intensities go to zero. This result can be easily understood by a co-ordinate transformation into either the principal axes of the EFG, or along the direction of the magnetic field with a new projection axis z'. If this is done, I_z is again a good quantum number, and the selection rules forbid transitions between the states $m' = \pm 3/2 \rightarrow m = \mp 1/2$. However, when the EFG and the magnetic field both contribute appreciably, then all possible transitions are allowed. The relative intensities vary in a fairly complicated way. Illustration 3 shows this variation for the range of the field strength ratio going between 0 and 2, which is the region of interest in the present investigations. The computer program which calculates the energies and the intensities is given in the appendix.

It is unfortunate that the eight peaks that are predicted cannot be observed experimentally. The reason for this is that the line widths and interaction energies which occur are of such sizes that the region of magnetic field strengths in which all eight intensities differ appreciably from zero is also the region in which all the peaks

ILLUSTRATION 3

The relative transition intensities from the four hyperfine levels of the excited nuclear state to the two hyperfine levels of the ground state: the wave functions shown, which specify the ground state levels are written in the representation for which the magnetic field is along the x-axis. The labels on each of the curves indicate the excited state level involved in the transition, and are the same as the labels used in Illustration 2. Note that the physical system has azimuthal symmetry, so that the choice of the x-axis is arbitrary.

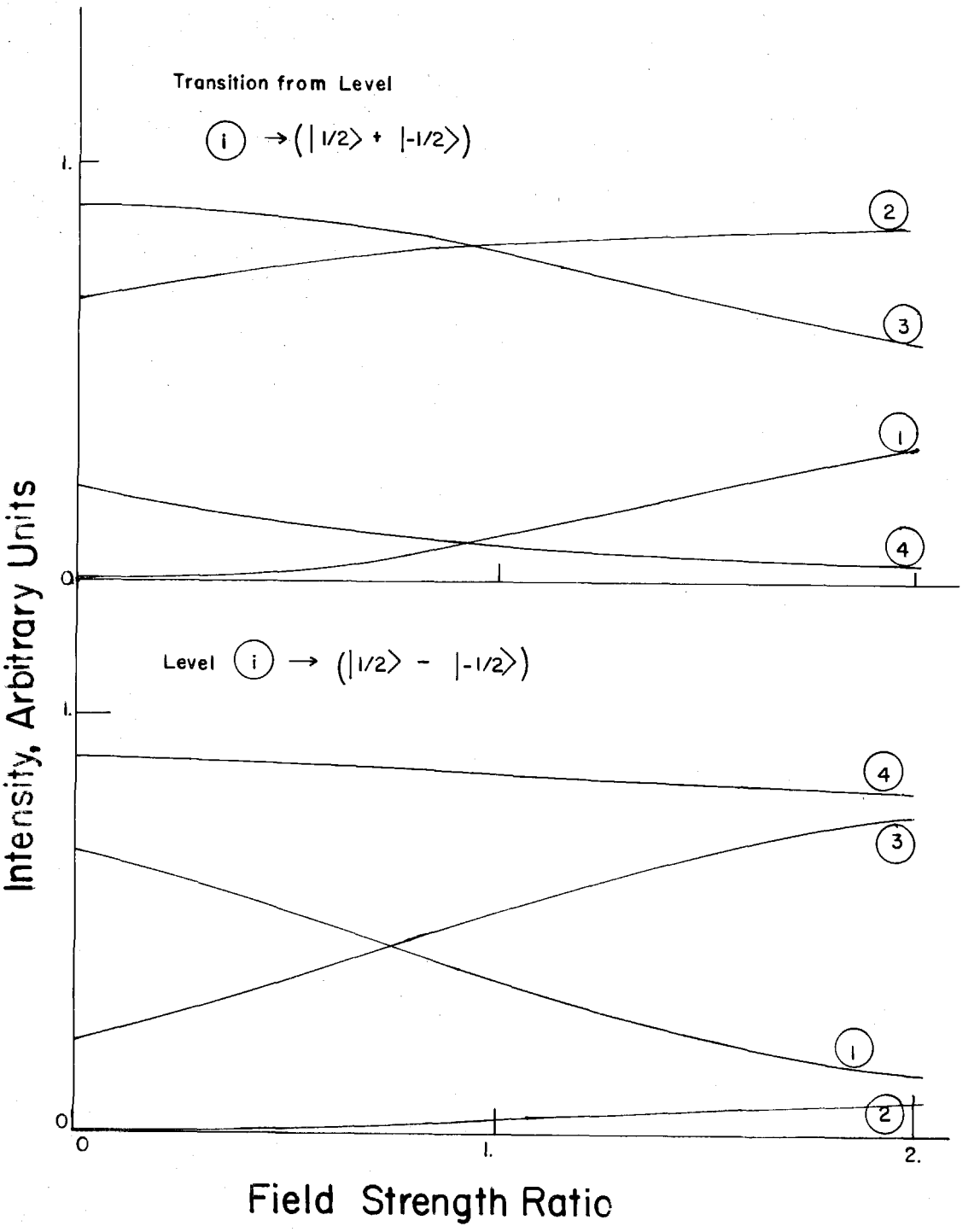
Transition from Level
(i) → (|1/2⟩ + |-1/2⟩)
1.
0
2
3
1
4
Level (i) → (|1/2⟩ - |-1/2⟩)
1.
0
4
3
1
2
0
1.
2.
Intensity, Arbitrary Units
Field Strength Ratio

are separated by an amount smaller than, or comparable to, the line width. For field strengths which are large enough to lead to a well-resolved pattern of lines, two of the intensities vanish, producing a six-peak pattern.

The data are taken with the apparatus described in the next chapter. The field strength effects were determined by a least-squares fit, with the aid of the digital computer. The positions of the peaks are determined by rewriting the hamiltonian for the nuclear excited state (Equation 18) in the form (with field in the x-direction)

$$H = Q/6\,[3I_z^2 - I(I+1) + WI_x]\,. \tag{21}$$

With this form the energies of the excited state become

$$E_i = (Q/6)\,f_i(W)\ , \tag{22}$$

so that, for $W = 0$, Q measures the quadrupole splitting directly, in units of cm/sec. A comparison with Equation (18) shows that

$$QW/6 = \frac{g_e \mu_N}{I} H_{int}\ , \tag{23}$$

in units of cm/sec. From Equations (23) and (10), we obtain H_{int} and $\langle r^{-3} \rangle_M$.

V. EXPERIMENTAL APPARATUS

The experiments reported on here were performed with the absorber at temperatures ranging from 3 ^{o}K up to 77 ^{o}K. The source was anhydrous ErF_3 heated in a holder of special design to a temperature of 275 ^{o}C; the holder was attached to a transducer drive so that the relative velocity of source and absorber could be varied. The details of the preparation of the sources and of the construction of the holder have been reported elsewhere[1].

The absorbers were mounted in a cryostat of special design, the essential features of which are shown in Illustration 4. The cryostat was mounted so that the absorber was located between the poles of an electromagnet.

Radiation passes into the absorber holder through a beryllium window mounted on the outside of the outer vacuum enclosure. It then passes through another beryllium window soldered into a copper box which is in good thermal contact (via a copper pipe) with the liquid nitrogen shield. Thus, thermal radiation is effectively blocked from the absorber holder area, while the gamma radiation passes in easily.

The absorber is mounted between beryllium discs in a copper block which is held in good thermal contact with the variable temperature tail, which acts as a connection of widely varying thermal conductance between the helium reservoir and the absorber holder. Heat transfer is controlled by gas pressure in the tail (this gas is called "exchange gas"; it is also helium, but comes from an independent supply). The highest temperature is, of course, obtained when the exchange gas is entirely removed; and it varies downward in a smooth way as the pressure is raised. Provisions were made for

ILLUSTRATION 4

A cross-section view of the cryostat used in the experiments. The pole of the electromagnet is centered over the center of the absorber space.

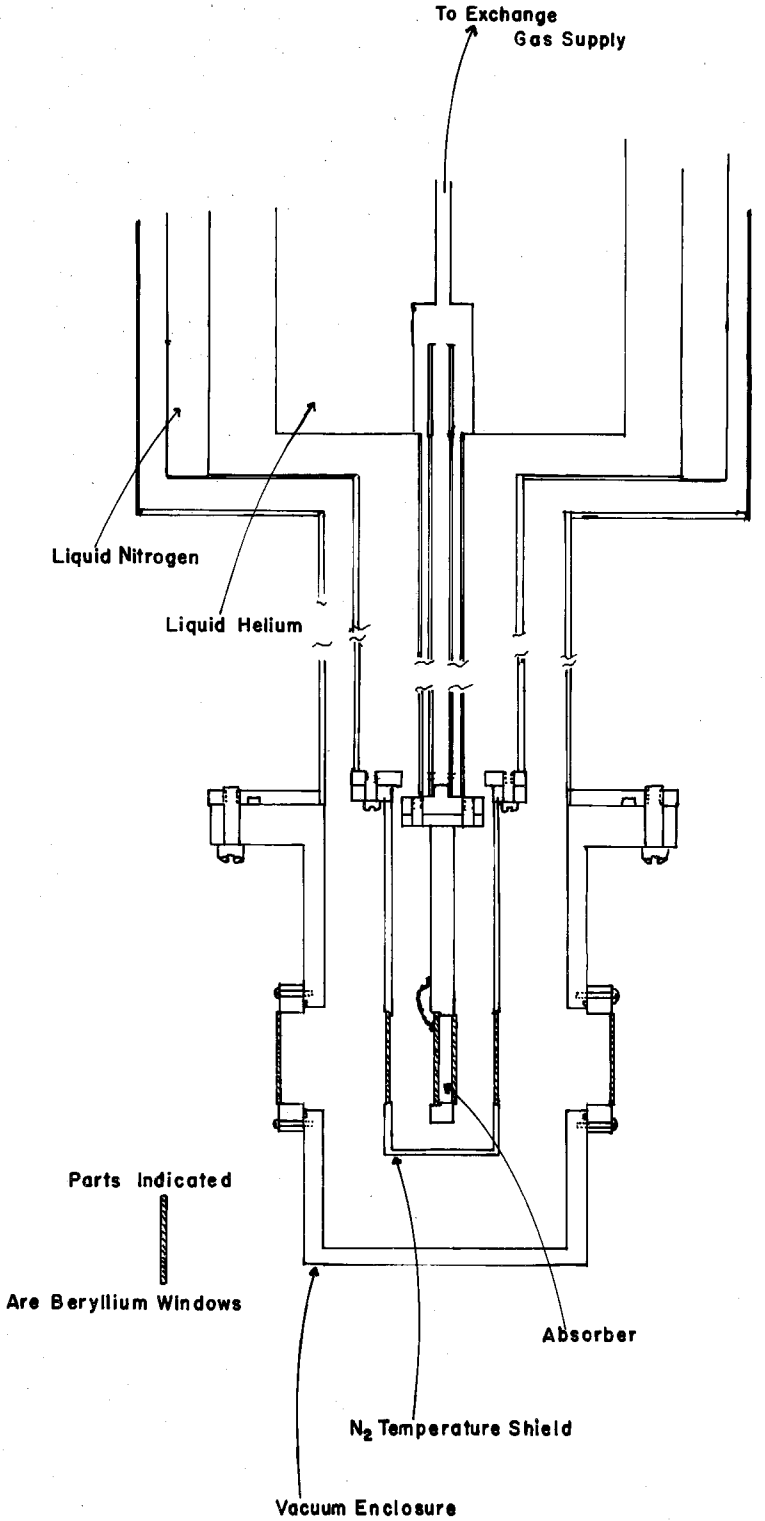
To Exchange
Gas Supply
Liquid Nitrogen
Liquid Helium
Parts Indicated
Are Beryllium Windows
Absorber
N_2 Temperature Shield
Vacuum Enclosure

supplementary electrical heating of the absorber holder, for more precise control of the temperature. However, it has never been found necessary to use any heating, since the pressure regulation alone sufficed for sufficiently accurate and stable control. Pressure is controlled by a system of valves, of which a schematic diagram appears in Illustration 5.

Temperature is measured with carbon resistors and with a copper-constantan thermocouple. The thermocouple is used only for relatively high temperatures, (40 ^{o}K and higher), since the thermoelectric power becomes inconveniently small as the junction becomes colder. The carbon resistors, on the other hand, become increasingly sensitive as the temperature is lowered, and are quite satisfactory at temperatures of 40 ^{o}K and lower. The overlap of useful ranges of temperature measurement makes it possible to compare the sensing devices with each other.

The carbon resistors were calibrated by immersion in cryogenic liquid (helium, hydrogen, and nitrogen) while the resistance was measured. The known temperatures and resistances were then used to determine the constants in a semi-empirical formula[6], which has been found to fit the behavior of the resistors quite well. The use of this formula:

$$\log R + \frac{A}{\log R} = \frac{B}{T} + C \ , \qquad (24)$$

where R is resistance, T is absolute temperature, and A, B and C are constants, permits one to avoid the formidable experimental problem of determining the value of resistance at enough temperatures to make an accurate freehand graph (or numerical table) of the variation.

ILLUSTRATION 5

The exchange gas pressure regulator. Valve no. 1 is a micrometer screw controlled needle valve (Whitey type number 22RVS4). The remaining valves are all conical seat globe valves of relatively high conductance (Whitey type number LVS4).

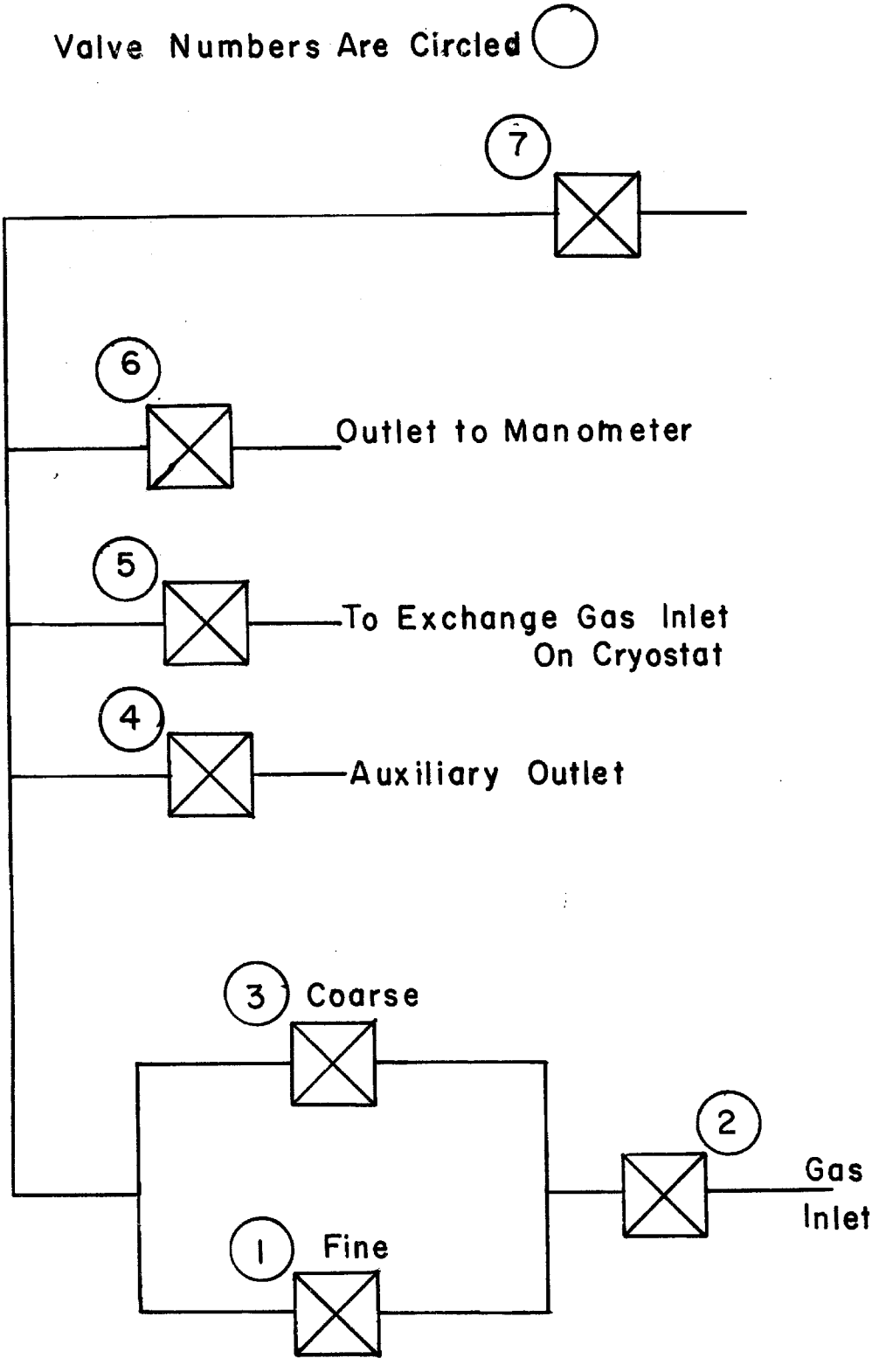
Valve Numbers Are Circled
7
6
Outlet to Manometer
5
To Exchange Gas Inlet
On Cryostat
4
Auxiliary Outlet
3
Coarse
2
Gas
Inlet
1
Fine

The stability of the resistors with respect to both thermal cycling and magnetic fields has proved excellent. No significant change in resistance has been observed when the resistors were recalibrated. It should be pointed out however, that the resistors have been used in relatively "mild" conditions. The temperature was varied slowly, and the resistors have always been used while in the insulating vacuum of the cryostat.

The drive system is illustrated in the semi-schematic diagram shown in Illustration 6. The multichannel analyzer operates in "multiscaler" mode: i. e., counts from the detector are stored in a particular channel of the analyzer for a preset period of time (either 200 or 400 microseconds for these experiments). The analyzer is then turned off, the channel number is changed to the next higher one, and the next channel is then opened to accept counts for the same preset time. This process of advancing channel number and gating the analyzer on and off is controlled by an external pulse generator, operating at fixed frequency. The velocity generating system is synchronized with the channel number by means of a bistable circuit which supplies a positive output voltage whenever the analyzer is operating in (say) channels No. 0 to 199, and negative output voltage whenever the analyzer is operating in (say) channels No. 200 to 399. This alternating voltage is made into an accurate square wave, integrated one or two times, and used as a velocity reference signal. A feedback control system causes the drive to have a velocity which varies in the same way with time as the reference voltage.

It is clear that in this system, a particular velocity of the drive corresponds exactly in time to a particular channel setting. Progressive variations in phase cannot occur, since exact synchronism

ILLUSTRATION 6

A semi-schematic diagram of the drive system used. All amplifier symbols except for the one in the line feeding the drive coil refer to low power level, high gain, operational amplifiers. The amplifier symbol preceding the drive coil actually represents a combination of an operational amplifier with the low gain, high power, amplifier shown in Illustration 7.

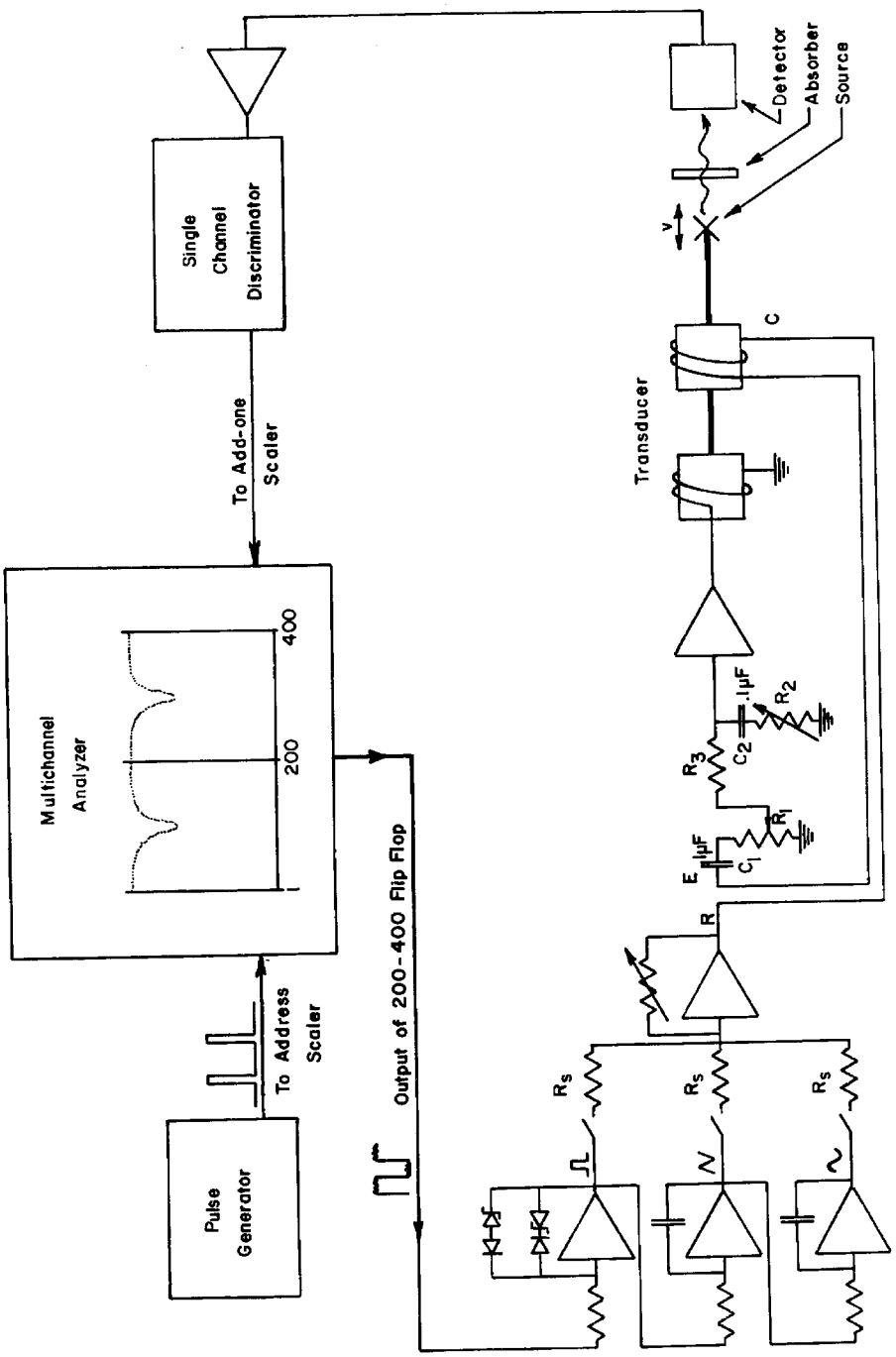
Detector
Absorber
Source
v
C
Transducer
R
E
1μF
C1
R1
R3
C2
.1μF
R2
Rs
Rs
Rs
Single Channel Discriminator
To Add-one Scaler
Multichannel Analyzer
400
200
Output of 200-400 Flip Flop
To Address Scaler
Pulse Generator

is restored twice in each cycle. One can also use any velocity variation with time that one wishes, provided that sufficiently complicated electronic networks are used to generate the appropriate waveforms from the input rectangular wave.

The electromechanical drive system consists of drive and pickup coils moving in separate ring-gap permanent magnets. Both coils are rigidly attached to a central shaft; the heated source holder is attached to the end of the shaft, and the whole assembly is mounted on cantilever springs. This constituted a mechanical resonant system, whose fundamental frequency has been adjusted to approximately 12 H_z. For further details of the design of the drive and electronics, see references 7 and 8.

For the experiments reported on here, velocities with either a triangular or parabolic variation with time (obtained by integrating the reference square wave once or twice) were used. The triangular velocity variation has the advantage that the observed spectra are easy to interpret; velocity is a linear function of channel number. However, the feedback control system does not accurately reproduce triangular variations of large amplitude. The high frequency cutoff is necessarily limited in order to prevent spontaneous oscillations, and the voltage gain must be kept low enough that the feedback amplifiers will not saturate. Accordingly, it is desirable that the harmonic content of the velocity reference signal be small, and that the reference signal be relatively smooth so that "spikes" of large amplitude are not generated in the feedback network. These considerations are particularly important at high velocity; accordingly, a parabolic variation of velocity was used when maximum velocities were greater than approximately 6 cm/sec. The "error signal"

(deviation of the pickup signal from the reference signal) was typically a factor of 5 smaller for the parabolic variation at the higher velocities.

In order to operate at the highest velocities, the feedback system must deliver considerable power to the drive coil. Commercial power amplifiers do not have adequate low frequency characteristics, so an audio amplifier shown in Illustration 7 was designed and built. This amplifier is DC coupled, has a voltage gain of about 8, a high frequency cutoff of about 10 kHz, and delivers an ampere into a 50 ohm load. Since there are no networks to stabilize the amplifier against DC drift, it is necessary to balance the output voltage level occasionally. The long-term drift has not been found to exceed about five volts per month, so the drift is not a serious problem. In order to prevent burning out the drive coil in case of sudden failure of one of the transistors, the output may be fused.

ILLUSTRATION 7

A schematic diagram of the power amplifier used. All resistors are 1 W, 5% unless otherwise specified. The "balance" switches are used to short-circuit the inputs to each state while the output voltage is adjusted to zero.

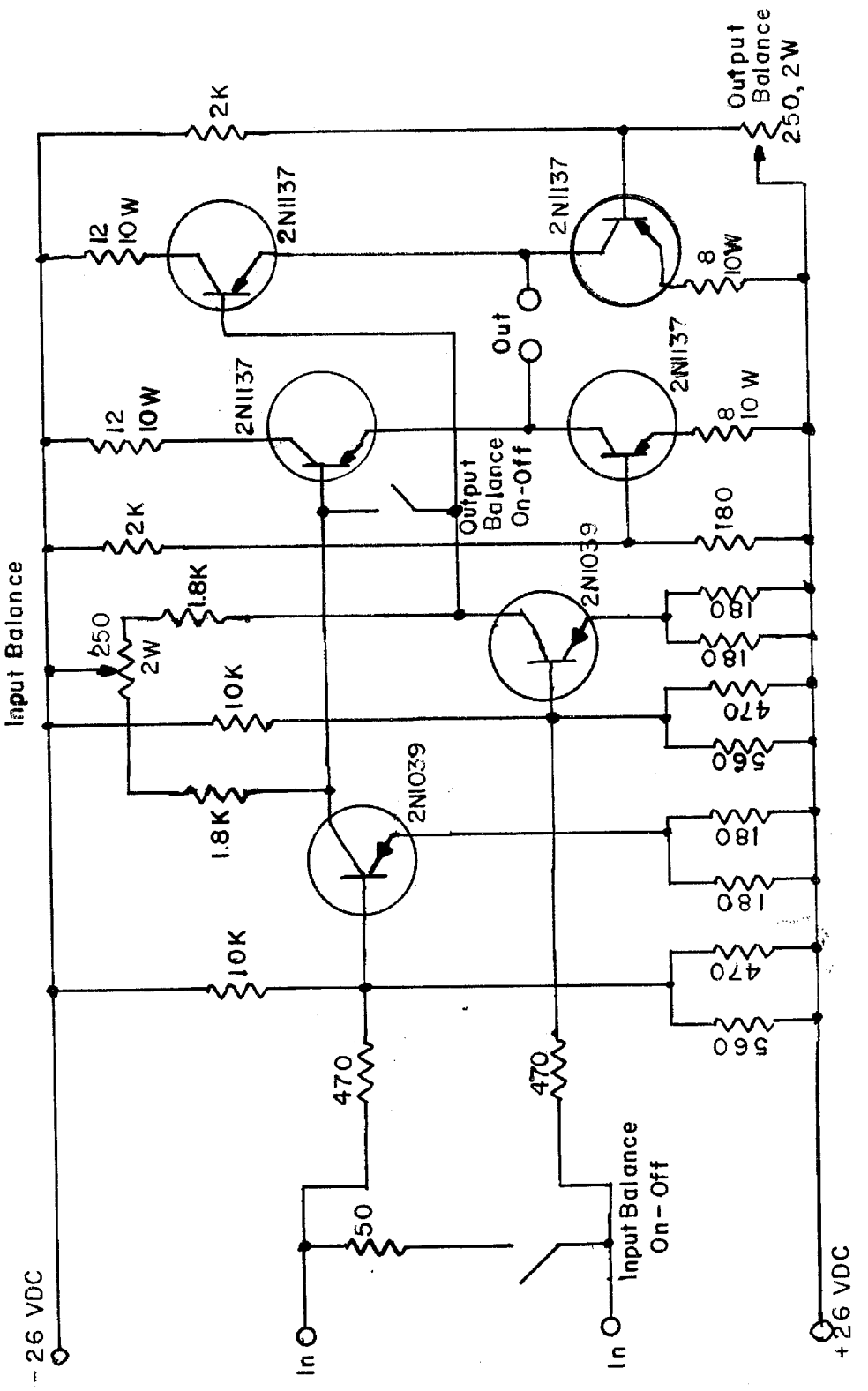
2K
12 10W
2N1137
2N1137
Output Balance 250, 2W
8 10W
Out
2N1137
2N1137
12 10W
8 10W
Output Balance On-Off
2K
180
2N1039
Input Balance
250 2W
1.8K
180
180
10K
470
560
2N1039
1.8K
180
180
10K
470
560
470
470
50
Input Balance On-Off
In
In
-26 VDC
+26 VDC

VI. RESULTS AND CONCLUSIONS

Several single crystals of thulium ethylsulphate were obtained. They varied in volume from approximately 1/2 cm^3 up to 3 or 4 cm^3. One of these, in the form of a hexagonal prism with dimensions approximately 2 mm x 4 mm x 25 mm was examined by x-ray techniques. The Laué transmission pattern confirmed the assignment of the symmetry classification (class C_{6h}), and showed that the hexagonal axis was parallel to the long axis of the crystal used. The crystal was then sawed by a string saw lengthwise into three slabs, each of approximate width 0.6 mm, and these slabs were then glued to a 2.54 cm diameter beryllium disc. The resulting mounted array was then ground on dry sandpaper followed by wiping with a damp towel until the final thickness was approximately 0.1 mm.

The absorber was placed in the cryostat discussed in the previous section. Since the rare earth ethylsulphates are quite prone to lose water of hydration in vacuum at room temperature[9], great care was taken to be sure that the absorber was quite cold (close to liquid nitrogen temperature) before the cryostat was pumped out. The absorber temperature was never allowed to rise above liquid nitrogen temperature during the experiments, and precautions were always taken to be sure that some liquid nitrogen remained in the cryostat when it was vented to atmospheric pressure. The absorber was in good condition after the experiments. It retained the clear pale green appearance characteristic of the single crystal TmES, indicating that chemical decomposition did not occur.

Spectra were taken for a variety of field strengths parallel and perpendicular to the hexagonal axis. The results illustrated in Illustration 8 indicate the anisotropy of the internal field, which was

ILLUSTRATION 8

Spectra taken with 1500 gauss perpendicular to the hexagonal axis, and 13,000 gauss parallel to the hexagonal axis. For a zero field spectrum, see Illustration 1.

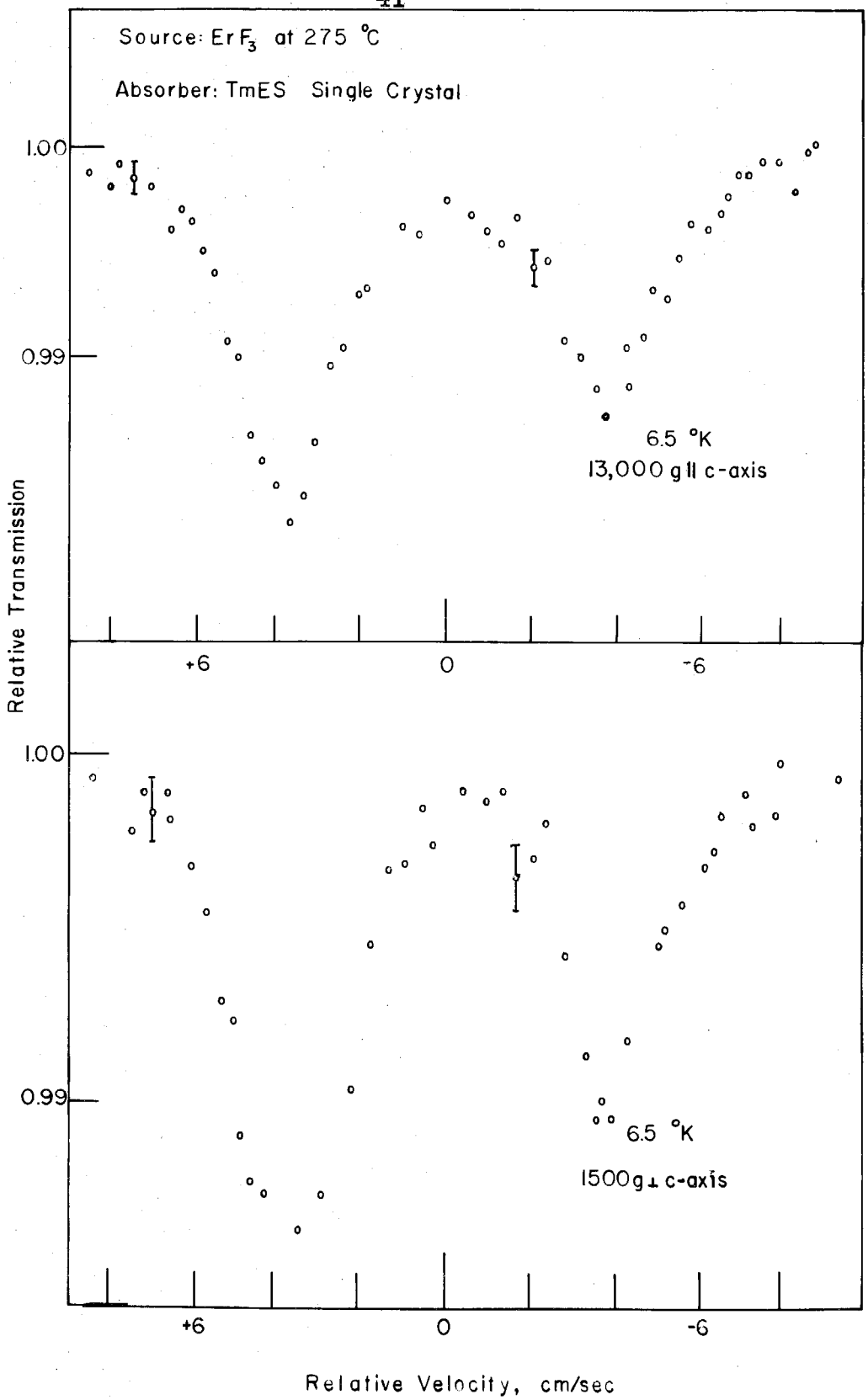
Source: ErF_3 at 275 °C
Absorber: TmES Single Crystal
1.00
0.99
6.5 °K
13,000 g ll c-axis
+6
0
-6
1.00
0.99
6.5 °K
1500 g ⊥ c-axis
+6
0
-6
Relative Transmission
Relative Velocity, cm/sec

also mentioned in Chapter III, in a striking way. A parallel field of 13 kilogauss does not give any magnetic field effect that we can see. If we assume the magnetic field effects to be about 10% of the line width, which is about the smallest effect that can be readily seen, we compute an upper limit of about 25 kilogauss for the internal field, which is a field strength about twice as large as that which is applied externally. A spectrum taken with a perpendicular field of 1.5 kilogauss (which is the smallest field that can be produced with the magnet used) is included to illustrate that a magnetic field effect is readily discernable with even a relatively small field in the perpendicular direction.

We obtained our quantitative results with a larger perpendicular field of 5850 gauss, at a temperature of 6.5 ^{o}K. The data were fit to eight Lorentz peaks whose relative amplitudes and positions were determined by the methods described in Chapter IV. The widths of the individual peaks were taken to be the same, and the magnitude of the width was left as a parameter. The width, along with the quadrupole splitting and the field intensity ratio, were varied to obtain a least-squares fit to the data. For smaller external fields, the line width correlated so strongly with the field intensity ratio that the fit was very poor, and tended to produce unreasonably small line widths in the final result. The results of the fit for the case of 5850 gauss are shown in Table 2; the errors are statistical only.

The fitted function is shown in illustration 9, superimposed on the experimental data points; a parallel field fit (in which the internal field was found to be zero) is shown for comparison.

ILLUSTRATION 9

Spectra taken with about 5000 gauss parallel to the hexagonal axis, and 5850 gauss perpendicular to the hexagonal axis. The solid curve is the calculated curve obtained from the parameters in Table 2, p. 43.

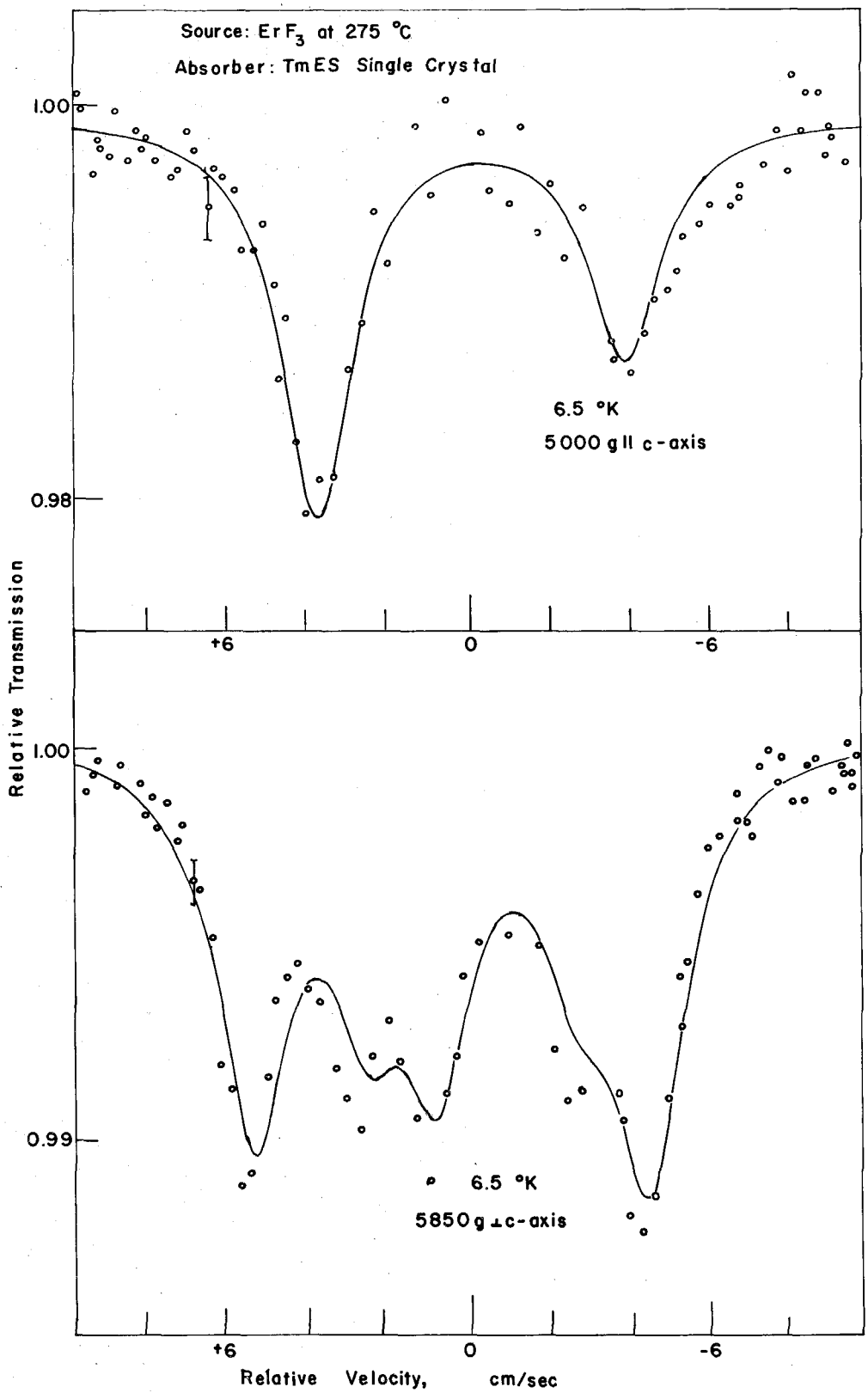
Source: ErF_3 at 275 °C
Absorber: TmES Single Crystal
1.00
0.98
6.5 °K
5000 g ll c-axis
+6
0
-6
Relative Transmission
1.00
0.99
6.5 °K
5850 g ⊥ c-axis
+6
0
-6
Relative Velocity, cm/sec

TABLE 2

Fitted to run with 5850 gauss at 6.5 ^{o}K

Parameter	Value
Line Width	1.31 ± 0.25 cm/sec
Q	7.871 ± 0.20 cm/sec
Field Ratio = W	1.23 ± 0.07 dimensionless

A separate fit was made with the line width constrained to be 2.0. The results for Q and W remained within the error limits. From these data we obtain an internal field of $(4.31 \pm 0.5) \times 10^5$ gauss (taking the g-factor of the excited state of thulium to be 0.50 ± 0.02 nm)[11]. This can be compared with the external field of 5.85×10^3 gauss, which implies an enhancement of the external field by a factor of 73 ± 7. We may now compare this enhancement factor with our upper limit of 2 for the parallel case. The ratio of enhancement factors, the internal field anisotropy A, is then seen to be $A \gtrsim 35$, which is in reasonable agreement with the value of A = 30 derived from susceptibility measurements[10], and is consistent with the theoretically calculated value of 50.

From the value of the internal field calculated above, we can now calculate $\langle r^{-3} \rangle_M$. The theoretical value of $\langle J_x \rangle$, at zero temperature, with the external field used is 0.4. The value obtained from the susceptibility measurements of Gerstein et al. is 0.39 at 6.5 ^{o}K. Using the theoretical value of $\langle J_x \rangle$, we obtain $\langle r^{-3} \rangle = 11.1 \pm 1.0$ atomic units.

This value may be compared with other theoretical and experimental determinations. Various calculations of the electronic wave functions for the rare earths have led to estimates of $\langle r^{-3} \rangle_M$ which are in disagreement with each other by as much as 30%. However, Bleaney[12] has found that the ratio of $\langle r^{-3} \rangle_M$ for the neutral rare earth atom to $\langle r^{-3} \rangle_M$ for the tripositive ion is in good agreement with the theoretical calculations of Judd and Lindgren[13] for all the cases in which reliable measurements are possible. Since $\langle r^{-3} \rangle_M$ for neutral thulium has been determined with considerable precision by atomic beam techniques[14], it is possible to estimate $\langle r^{-3} \rangle_M$ for the ion with some confidence. In Table 3, we compare experimental and theoretical values of $\langle r^{-3} \rangle_M$ for thulium.

TABLE 3

Values of the $\langle r^{-3} \rangle_M$ for Tm^{IV}

Source	Value (atomic units)	Method
Freeman and Watson[15]	12.9	Hartree-Fock (coulomb value)
Judd and Lindgren	10.95	Modified hydrogenic
Bleaney	11.72	ratio to Tm^{I} exptl. value.
Cohen[11]	12.5 ± 0.7	Mössbauer Effect in Fe_2Tm
This work	11.1 ± 1.0	Mössbauer Effect in TmES

The experimental values quoted here are not precise enough to clearly distinguish among the various theoretical values. If the difference between the present result and that of Cohen is considered to be meaningful, it is then possible to remark that the presence of polarized conduction electrons tends to enhance the internal field. It is, however, clearly necessary to perform further experiments before the matter can be settled unambiguously. The statistical error in the present measurement is rather large. In order to obtain a more precise result, an experiment using a superconducting magnet is planned. With the much larger magnetic field which can be obtained in this way, it should be possible to determine the internal field with considerable precision, and to infer with some confidence the variation, if any, of the value of $\langle r^{-3} \rangle_M$ as the chemical binding changes from ionic to metallic.

The emphasis in the discussion above has centered in the measurement of the magnetic hyperfine interaction. However, it should be pointed out that other quantities of physical interest may be determined by studies on single crystals. A few of these are enumerated below:

(1) Mössbauer experiments with a polycrystalline aggregate salt can give only the magnitude of the product of the EFG with the quadrupole moment of the nucleus. The application of a magnetic field does not materially improve one's knowledge of the situation, since the observed result is an average over all orientations, which may be quite difficult to interpret. However, the application of a magnetic field to a single crystal can give the sign of the product unambiguously, even when precise details of the atomic electron structure are not known; it suffices to apply the field in one of the principal directions of the magnetic susceptibility tensor, so that

the direction of the internal field with respect to the EFG axes is known. For example, we find that $Q < 0$, for the excited state of Tm^{169}, which is consistent with theoretical predictions from the collective model.

(2) Measurements such as these are useful as a supplement to bulk susceptibility measurements, especially when the bulk measurements are likely to be in error due to small inclusions of impurities, or when the susceptibility of a particular atomic species in a mixed material is desired. In contrast to bulk susceptibility measurements, a fraction of a per cent impurity content does not seriously interfere with Mössbauer measurements, since the spectra of such a small fraction of all atoms present would be unobservable in the background. The present experiments indicate one instance of this, since the anisotropy observed here is slightly larger than the anisotropy determined from the susceptibility measurements, which may, according to Gerstein et al.[10], be in error due to missing water of hydration.

(3) The internal field is considerably higher than the external field, by a factor of about 75 in our case. While it is not too surprising that field should be so large, there seems to be little use made of this fact in areas of investigation such as nuclear alignment or nuclear demagnetization, where a large nuclear magnetic interaction is desired. The field enhancement factor is large enough in our case that a quite appreciable difference in nuclear substate populations could be achieved at temperatures which can be reached fairly readily. The importance of our results and techniques is first the realization that such large fields are relatively easy to achieve, and second that an experimental technique for the measurement of these fields is available.

BIBLIOGRAPHY

1. R. G. Barnes, R. L. Mössbauer, E. Kankeleit and J. M. Poindexter, Phys. Rev. 136, A175 (1964).

2. R. J. Elliott and K. W. H. Stevens, Proc. Roy. Soc. (London) A218, 553 (1953).

3. See, e. g. A. Abragam, Nuclear Magnetism, Clarendon Press, Oxford (1961).

4. L. W. McKeehan, Phys. Rev. 43, 1025 (1933).

5. M. E. Rose, Multipole Fields, John Wiley and Sons, New York (1955).

6. J. R. Clement and E. H. Quinnel, Rev. Sci. Inst. 23, 213 (1952).

7. E. Kankeleit, Rev. Sci. Inst. 35, 194 (1964).

8. E. Kankeleit, to be published in Advances in Mössbauer Effect Methodology, Plenum Press, New York, (1965).

9. Lorin Vant-Hull, private communication.

10. B. C. Gerstein, L. D. Jennings and F. H. Spedding, Jour. Chem. Physics 37, 1496 (1962).

11. R. L. Cohen, Phys. Rev. 134, A94 (1964).

12. B. Bleaney, Proceedings of the Third International Conference on Quantum Electronics, Columbia University Press, New York (1964), p. 595.

13. B. R. Judd and I. Lindgren, Phys. Rev. 122, 1802 (1961).

14. G. J. Ritter, Phys. Rev. 128, 2238 (1962).

15. A. J. Freeman and R. E. Watson, Phys. Rev. 127, 2058 (1962).

APPENDIX 1

This program calculates the hyperfine energies and transition intensities to the sublevels of the ground state when a magnetic field in the x-direction is present. The methods of Chapter IV are used.

```
      SUBROUTINE INT(W,B1,B2,EN)
C     PROGRAM TO CALCULATE THE ENERGIES AND INTENSITIES OF THE
C     I = 3/2 STATE WHEN THE MAGNETIC FIELD IS PERPENDICULAR
C     TO THE C-AXIS
C     W = FIELD STRENGTH RATIO.  B1,2 = INTENSITIES FROM A
C     HYPERFINE STATE TO -,+ IN THE GROUND STATE
C     EN = ENERGIES OF THE HYPERFINE STATES
      DIMENSION B1(4),B2(4),EN(4)
      REAL INTNS
      REAL M, MPRIM
      INTEGER DIFF
      DIMENSION A(4,4), V(4,4), EIGV(4), BLANK(35)
      ROOT = 1./SQRT(3.)
       DO 10 I = 1,4
      DO 10 J=1,4
      A(I,J) = 0.0
      V(I,J) = 0.0
   10 CONTINUE
      DO 11 I = 1,4
      DO 11 J = 1,4
      M = FLOAT(I) - 2.5
      MPRIM = FLOAT (J) - 2.5
      DIFF = I - J
      IF (DIFF - 0) 31,30,31
   30 A(I,J)= 3.*M**2 - 15./4.
      GO TO 11
   31 IF (DIFF - 1) 32,33,32
   33 A(I,J) = (SQRT((1.5 - MPRIM)*(1.5 + MPRIM + 1.)))*W
      GO TO 11
   32 IF (DIFF + 1) 11,34,11
   34 A(I,J) = (SQRT((1.5 +MPRIM)*(1.5- MPRIM + 1.)))*W
   11 CONTINUE
   51 CALL EIGVV(A,V,EIGV,4,BLANK  )
      DO 24 I = 1,4
   24 EN(I)  = EIGV(I)
   52 DO 12 I = 1,4
      F = -1
      II = 1
  203 X1 = 0.5*(V(4,I) + ROOT*V(3,I)*F - V(1,I)*F
     1 -ROOT*V(2,I))**2
      X2 = (2./3.)*(V(3,I) + V(2,I)*F)**2
      INTNS =(X1 + X2)/3.
      GO TO (201,202),II
  201 B1(I) = INTNS
      F = 1
      II = 2
      GO TO 203
  202 B2(I) = INTNS
   12 CONTINUE
      RETURN
      END
```